

Isoscaling of projectile-like fragments

C. Zhong, Y. G. Ma, D. Q. Fang, X. Z. Cai, J. G. Chen, W. Q. Shen, W. D. Tian, K. Wang,
Y. B. Wei, J. H. Chen, W. Guo, C. W. Ma, G. L. Ma, Q. M. Su, T. Z. Yan, and J. X. Zuo
Shanghai Institute of Applied Physics, Chinese Academy of Sciences, P. O. Box 800-204, Shanghai 201800, China
(dated: November 26, 2018)

The isotopic and isotonic distribution of the projectile fragmentation products have been simulated by a modified statistical abrasion-ablation (SAA) model and the isoscaling behavior of projectile-like fragments has been discussed. The isoscaling parameters and for hot fragments before evaporation and cold fragments after evaporation have been extracted, respectively. It looks that the evaporation has strong effect on . For cold fragments, a monotonic increase of and j with increase Z and N is observed. The relation between isoscaling parameter and the change of isospin content is demonstrated. In addition, the disappearance of the isospin effect of projectile fragmentation is also discussed in the viewpoint of isoscaling parameter.

PACS numbers: 25.70.Mn, 42.10.Pa

Recently, isoscaling behavior has been observed [1, 2, 3, 4]. The scaling law relates ratios of isotope yields measured in two different nuclear reactions, 1 and 2, $R_{21}(N; Z) = Y_2(N; Z)/Y_1(N; Z)$. In multifragmentation events, such ratios are shown to obey an exponential dependence on the neutron number N or proton number Z of the isotopes characterized by three parameters α , β , and C [1]:

$$R_{21}(N; Z) = \frac{Y_2(N; Z)}{Y_1(N; Z)} = C \exp(\alpha N + \beta Z); \quad (1)$$

In grand-canonical limit, $\alpha = \mu_n/T$ and $\beta = \mu_z/T$ where μ_n and μ_z are the differences between the neutron and proton chemical potentials for the two reactions, respectively. C is an overall normalization constant. This behavior is attributed to the difference of isospin asymmetry between two reaction systems in the similar nuclear temperature. It is potential to probe the isospin dependent nuclear equation of state [5, 6] by the studies of isoscaling [1, 2, 3, 4, 7, 8]. So far, the isoscaling behavior has been studied experimentally and theoretically for different reaction mechanisms. However, most studies focus on the isoscaling behaviors for light particles. A few studies on the heavy projectile-like residues in deep elastic collisions and fusion fragments have been reported [9, 10, 11, 12, 13]. In this paper, we concentrate our attentions on the isoscaling features in projectile fragmentation and discuss the effect of evaporation on the isoscaling parameters and in a framework of statistical abrasion-ablation (SAA) model [14].

Projectile fragmentation is one of the most important methods to produce beams of extreme neutron-rich or proton-rich nuclei and has been widely used to study nuclear reactions induced by heavy ions at intermediate and high energies. Various physical models for projectile fragmentation have been developed and the reaction mechanism

of heavy-ion collisions have been investigated extensively. For instance, an empirical parameterization, like EPAX/EPAX II formula presented by Summner et al. [15, 16], can predict the fragment production cross-section well. However, due to its poor physical foundation, the empirical parameterization may not be applicable in extrapolation. In addition, statistical abrasion-ablation model can describe the isotopic distribution well [14]. In the SAA model, the nuclear reaction is described in two stages which occur in two distinctly different time scales. The first abrasion stage is fragmentation reaction which describes the production of the prefragment with certain amount excitation energy through the independent nucleon-nucleon collisions in the overlap zone of the colliding nuclei. The collisions are described by a picture of interacting tubes. Assuming a binomial distribution for the absorbed projectile neutrons and protons in the interaction of a specific pair of tubes, the distributions of the total abraded neutrons and protons are determined. For an infinitesimal tube in the projectile, the transmission probabilities for neutrons (protons) at a given impact parameter b are calculated by [14]

$$t_k(r, b) = \exp[-D_N^T(r, b) \sigma_k^n + D_P^T(r, b) \sigma_k^p] g; \quad (2)$$

where D_K^T is thickness function of the target, which is normalized by $\int d^2r D_N^T = N^T$ and $\int d^2r D_P^T = Z^T$ with N^T and Z^T referring to the neutron and proton number in the target respectively, the vectors r and b are defined in the plane perpendicular to beam, and σ_k^0 is the free nucleon-nucleon cross sections (σ_k^0 , $k=n$ for neutron and σ_k^0 , $k=p$ for proton). The thickness function of the target is given by

$$D_K^T(r) = \int_1^{Z+1} dz \rho_K((r^2 + z^2)^{1/2}); \quad (3)$$

with ρ_k being the neutron (proton) density distribution of the target. So the average abraded mass at a given

Corresponding author. Email: ygm a@ sinap.ac.cn

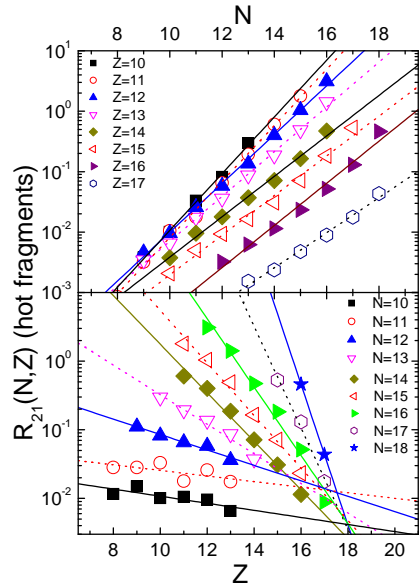


FIG. 1: Yield ratios $R_{21}(N;Z)$ of pre-fragments (also called hot fragments in this work) from the reactions of $^{40}\text{Ar} + ^9\text{Be}$ and $^{36}\text{Ar} + ^9\text{Be}$ at 60 MeV/nucleon versus N (top panel) or Z (bottom panel). The lines represent the exponential fits.

in fact parameter b is calculated by the expression

$$h(A, b) = \frac{R}{R} \frac{d^2 r_D}{d^2 r_D} \frac{P}{P} (r) [1 - t_n(r, b)] + \frac{d^2 r_D}{d^2 r_D} \frac{P}{P} (r) [1 - t_p(r, b)] \quad (4)$$

And the excitation energy of projectile spectator is estimated by a simple relation of $E^* = 13.3 h(A, b) \text{ MeV}$ where 13.3 is a mean excitation energy due to an abraded nucleon from the initial projectile [17]. In the second evaporation stage the system reorganizes due to excitation, which means it deexcites and thermalizes by the cascade evaporation of light particles. By inducing in-medium nucleon-nucleon cross section and optimizing computational method proposed by our group given in Ref. [18, 19, 20, 21], it can give a good agreement with the isotopic distribution at both high and intermediate energies involving neutron-rich or proton-rich nuclei over a wide energy range [18, 19, 21].

Fragment products have been measured at the Radioactive Ion Beam Line in Lanzhou using beams of 55 MeV/nucleon ^{40}Ar and 69 MeV/nucleon ^{36}Ar which were delivered by the Heavy Ion Research Facility in Lanzhou (HIRFL) to bombard on ^9Be target and the isospin effects on the isotopic distribution have been investigated. More details can be found in Refs. [18, 19]. The experimental results were well compared with the calculation of the modified statistical abrasion-ablation model which was originally developed by Brohm et al. [14].

From the simulation by SAA model, we extract the yield ratio $R_{21}(N;Z)$ using the convention that index 2 refers to the more neutron-rich system ($^{40}\text{Ar} + ^9\text{Be}$) and

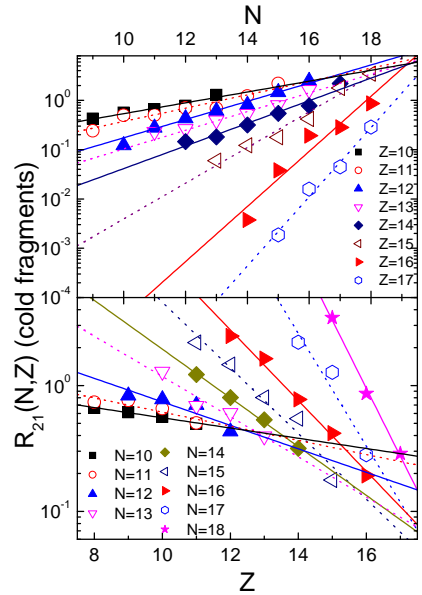


FIG. 2: Yield ratios $R_{21}(N;Z)$ of cold fragments from the reactions of $^{40}\text{Ar} + ^9\text{Be}$ and $^{36}\text{Ar} + ^9\text{Be}$ at 60 MeV/nucleon versus N (top panel) or Z (bottom panel). The lines represent the exponential fits.

index 1 to the less neutron-rich one ($^{36}\text{Ar} + ^9\text{Be}$). Figure 1 shows the yield ratios $R_{21}(N;Z)$ of hot projectile-like fragments (PLFs) as a function of neutron number N for selected isotopes (upper panel) and proton number Z for selected isotones (lower panel) for the $^{40-36}\text{Ar} + ^9\text{Be}$ reactions in the semi-log plots. In Figure 2, the corresponding ratios for the cold projectile-like fragments are shown in the semi-log plots. In the figures, the different isotopes and isotones are shown by alternating filled and open symbols for clarity. Even isotopes and isotones are shown with filled symbols, and odd ones are shown with open symbols.

From the upper panels of Fig. 1 (hot fragments) and Fig. 2 (cold fragments), we observe that the ratio for each isotope Z (from 10 to 17) exhibits a remarkable exponential behavior. For each isotope (Z), an exponential function form $C \exp(N)$ was used to fit the calculation points and the parameters are shown in the top panel of Fig. 3 for the selected Z . A analogous behavior is observed in the lower panels of Figs. 1 and 2, for each isotone (N), an exponential function form $C^0 \exp(Z)$ was used to fit the calculation points and the parameters are shown in the lower panel of Fig. 3 for the selected N .

The model predicts that the fragment isotopic distribution at a fixed atomic number Z shifts towards the neutron-rich side for the neutron-rich projectile. In Fig. 3, we present the slope parameters α (upper panel) and β (lower panel) of the exponential fits obtained as described for Figs. 1 and 2 as a function of Z and N , respectively. In the upper panel of Fig. 3, of the pre-fragments for each element show a little bit decreasing

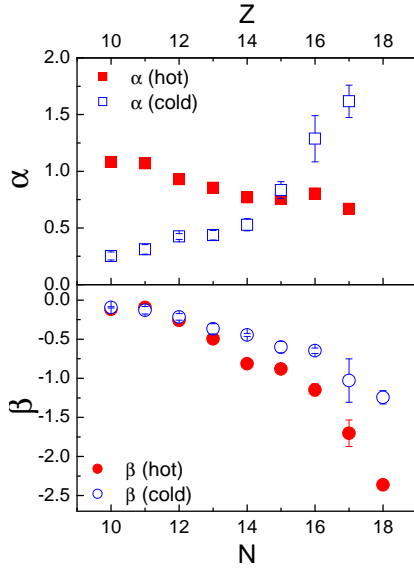


FIG. 3: Isoscaling parameters α as a function of Z (top panel) and β as a function of N (lower panel) for projectile fragmentation from the reactions $^{40}\text{Ar} + ^9\text{Be}$ and $^{36}\text{Ar} + ^9\text{Be}$ at 60 MeV/nucleon. Solid symbols represent the pre-fragments and open symbols represent final fragments.

trend with the increasing of Z . But, a monotonic increase of j with increasing N is observed. For cold fragments after evaporation (open symbols of Fig. 3), a monotonic increase of α and j with increase Z and N , respectively, is observed. From the lower panel of Fig. 3, j always increase with the increasing of N for hot fragments or cold fragments and j of hot fragments tends to drop when evaporation is taken into account.

In Fig. 4, we demonstrate the centroid and width of the isotopic distributions of projectile-like fragments from both reactions as well as their differences for the cases of hot fragments (top panel) and of cold fragments (bottom panel). The values of the isotopic distribution width are approximately the same for hot fragments from both reactions, and the differences of centroid of two distributions are approximately a constant. After evaporation, the centroid becomes very close for two systems, especially for lower Z of PLFs while the widths of the isotopic distributions tend to decrease as the microcanonical statistical multifragmentation model predicts [3]. Both the differences of the centroid and the width of the distributions drop with the decreasing of Z , which reflects a strong evaporation effect on projectile-like fragments [22, 23]. In the evaporation stage, neutrons are emitted with the most important probability, the final cold fragments are more symmetric than their hot ancestors. However, the charged particle emission is less important. Since α is the isoscaling parameter in fixed Z and β is the isoscaling parameter in fixed N , so the neutron evaporation has the strongest effect on α while charged particle evaporation has less effect on α . That results in an obvi-

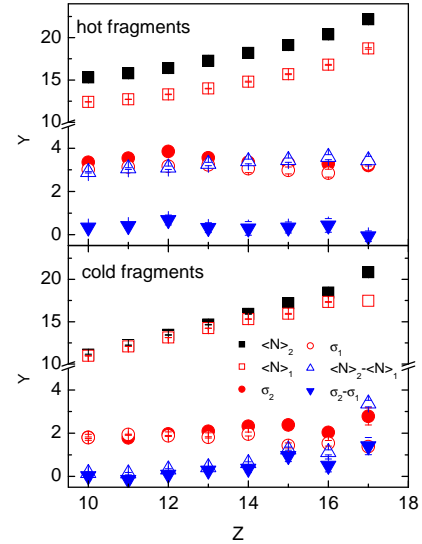


FIG. 4: The centroid ($\langle N \rangle$) and width (σ) of isotopic distributions for ^{40}Ar and ^{36}Ar system and their differences as a function of Z . The upper panel is for hot fragments and the lower panel is for cold fragments. The symbols are illustrated in insert.

ous change of α parameter while a weak change of β due to the evaporation.

In order to further discuss the reason of the dramatic change of the isoscaling parameters, we make a plot of $\langle N \rangle = Z$ versus Z in the upper panel of Fig. 5 for the fragments before and after evaporation. As we know, $\langle N \rangle = Z$ represents the isospin component. From the figure, the hot PLFs which are close to initial projectile basically remain larger isospin content as the initial projectile while lighter hot PLFs have much larger $\langle N \rangle = Z$ due to stronger dissipation and nucleon exchange. However, this high isospin content can not keep alive since the prefragments are excited as illustrated the above section. They will cool themselves by the light particle evaporation, mostly by the neutron emission. After the evaporation process, $\langle N \rangle = Z$ tends to 1.1 in lower Z and bifurcates in higher Z for ^{40}Ar and ^{36}Ar systems. More interestingly, we note that the differences of $\langle N \rangle = Z$ between two systems for hot and cold fragments as a function of Z as shown in the lower panel of Fig. 5. Consistently, this behavior is similar to α as a function of Z for hot and cold PLFs as shown in Fig. 3. In this context, we could say the difference of isospin content (i.e. the neutron-to-proton ratio: $\langle N \rangle = Z$) is a more simple measurement of isoscaling parameter α . Similar behavior has been found for j .

In the past years, the isospin dependence of various physical quantities has been reported [5, 19, 24, 25, 26, 27]. The positive slopes in the upper panels of Figs. 1 and 2 indicate that neutron-rich fragments are more efficiently produced, as expected, from the more neutron-rich systems. In other words, the fragment isotopic dis-

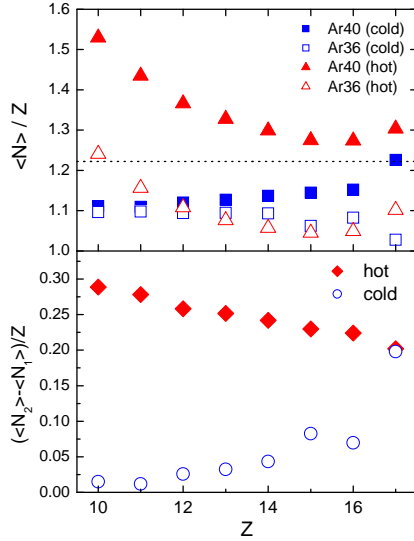


FIG. 5: (a) $\langle N \rangle / Z$ for hot and cold fragments for ^{40}Ar and ^{36}Ar systems. The dotted line is initial N/Z for ^{40}Ar ; (b) The differences of $\langle N \rangle / Z$ between ^{40}Ar and ^{36}Ar for the hot and cold fragments systems. The symbols are illustrated in insert.

tribution at a fixed atomic number Z shifts towards the neutron rich side for the neutron-rich projectile. This isospin effect will decrease with decreasing the fragment atomic number Z and disappear when $(Z_{\text{proj}} - Z) = Z_{\text{proj}}$ becomes larger [19]. The quantity of $(Z_{\text{proj}} - Z) = Z_{\text{proj}}$ can be related to excitation energy or temperature of the deformed projectile after the abrasion stage. When this quantity becomes smaller, the deformed projectile becomes hotter or highly excited. In this context, we can say that the isospin effect tends to fade out with the increasing of the excitation energy of the projectile-like system. In our work, as shown in the lower panel

of Fig. 4, the difference of the centroid and the width of the isotopic distribution becomes smaller as the decrease of Z (open up-triangles and solid down-triangles), and it approaches zero when projectile-like fragments are far away from the initial projectile Z_{proj} and becomes approximately zero. These pictures indicate that isoscaling parameters decrease with the excitation energy of the system [7] and isospin effect tends to vanish in high temperature [19, 24].

In summary, the isoscaling of projectile-like fragments from $^{40=36}\text{Ar} + ^9\text{Be}$ at 60 MeV/nucleon has been studied by a modified statistical abrasion-ablation model. SAAM model can simulate well the isotopic distribution of PLFs of the systems. The isoscaling parameters and are extracted for the prefragments and final fragments. It has a dramatic change after evaporation. For hot PLFs, it shows a little bit stronger isospin effect for those highly excited small PLFs. However, this kind of stronger isospin effect for smaller PLFs can not survive due to much more neutron evaporation from these highly excited pre-PLFs. Finally, it shows weaker for these smaller PLFs while stronger for PLFs close to initial projectile. A monotonic increase of (j, j) with increase Z (N) is observed. This behavior can be easily explained by the difference of the isospin content of hot or cold PLFs between two systems as shown in Fig. 5. In this sense, isospin content can take a simple "isomere" as isoscaling parameter. In addition, the disappearance of the isospin effect of projectile fragmentation is also discussed in the viewpoint of isoscaling parameter.

This work was supported in part by the Major State Basic Research Development Program under Contract No G 200077404, the Chinese Academy of Sciences Grant for the Distinguished Young Scholars of National Natural Science Foundation of China (NNSFC), and NNSFC under Grant No 10328259, 10135030, 10405032, 10405033, 10475108 and the Shanghai Phosphor Program Under Contract Number 03QA 14066.

-
- [1] M. B. Tsang et al., Phys. Rev. Lett. 86, 5023 (2001).
 [2] M. B. Tsang et al., Phys. Rev. C 64, 041603 (2001).
 [3] M. B. Tsang et al., Phys. Rev. C 64, 054615 (2001).
 [4] A. S. Botvina, O. V. Lozhkin, and W. Trautmann, Phys. Rev. C 65, 044610 (2002).
 [5] V. Baran, M. Colonna, V. Greife, M. Di Toro, Phys. Rep. 410, 335 (2005).
 [6] Y. G. Ma and W. Q. Shen, Nucl. Sci. Tech. 15, 4 (2004).
 [7] Y. G. Ma et al., Phys. Rev. C 69, 064610 (2004).
 [8] W. D. Tian et al., Chin. Phys. Lett. 22, 306 (2005).
 [9] G. A. Souliotis et al., Phys. Rev. C 68, 024605 (2003).
 [10] W. A. Friedman, Phys. Rev. C 69, 031601(R) (2004).
 [11] M. Veselsky, G. A. Souliotis, M. Jandel, Phys. Rev. C 69, 044607 (2004).
 [12] K. Wang et al., Chin. Phys. Lett. 22, 53 (2005).
 [13] Y. G. Ma et al., ArXiv nucl-th/0412034.
 [14] T. Borchmann and K. H. Schmidt, Nucl. Phys. A 569, 821 (1994).
 [15] K. Sumner et al., Phys. Rev. C 42, 546 (1999).
 [16] K. Sumner and B. Blank, Phys. Rev. C 61, 34607 (1999).
 [17] J. J. Ginard and K. H. Schmidt, Nucl. Phys. A 531, 109 (1991).
 [18] D. Q. Fang et al., Chin. Phys. Lett. 18, 753 (2001).
 [19] D. Q. Fang et al., Eur. Phys. J. A 10, 0381 (2001).
 [20] X. Z. Cai et al., Phys. Rev. C 58, 572 (1998).
 [21] C. Zhong et al., High Energy Phys. Nucl. (in Chinese) 27, 39 (2003).
 [22] A. S. Goldhaber, Phys. Lett. B 53, 306 (1974).
 [23] Y. G. Ma et al., Phys. Rev. C 65, 051602R (2002).
 [24] M. L. Miller et al., Phys. Rev. Lett. 82, 1399 (1999).
 [25] J. F. Dempsey et al., Phys. Rev. C 54, 1710 (1996).
 [26] H. Muller and B. D. Serot, Phys. Rev. C 52, 2072 (1995).
 [27] Y. G. Ma et al., Phys. Rev. C 60, 024607 (1999).